



# Research on dust fugitive characteristics of mobile dust sources based on industrial bulk material transfer process

Hongfa Sun<sup>1</sup> · Zhengyu Li<sup>1</sup> · Jibo Long<sup>1</sup> · Fang Ruan<sup>1</sup>

Received: 10 February 2023 / Accepted: 19 January 2024 / Published online: 1 March 2024  
© The Author(s), under exclusive licence to Springer-Verlag GmbH Germany, part of Springer Nature 2024

## Abstract

The process of transferring and conveying bulk materials are common in industrial production, and the dust pollution is a problem of mobile dust sources due to the velocity of the dust source. Firstly, a physical model of mobile dust sources is established. Secondly, the accuracy of the pollution model is verified by the existing experimental data. Finally, the effects of dust source velocity, wind velocity and particle diameter on dust fugacity are analysed. The results show that the wind velocity has the greatest influence on dust diffusion, especially the wind velocity of 3 m/s; The influence of different dust source velocity on the spatial distribution of dust concentration mainly exists in the area near the mobile surface; For dust diameter less than 10 $\mu$ m, the diameter has little effect on dust diffusion. In order to describe the dust pollution situation, the dust initiation rate was defined to evaluate the dust intensity of each condition. The biggest influence is wind velocity. When the wind velocity is 0.5 m/s, the dust initiation rate is only  $2.5 \times 10^{-5} \text{ s}^{-1}$ . When the wind velocity reaches 10 m/s, the dust initiation rate is  $1.5 \times 10^{-4} \text{ s}^{-1}$ . The dust initiation rate increases with the velocity of mobile dust source. The results can provide theoretical basis for dust pollution control in the process of transporting industrial bulk materials.

**Keywords** Mobile dust sources · Bulk materials · Dust pollution · Dust initiation rate · Wind velocity

## 1 Introduction

The transportation of bulk materials is common in industrial production. The dust dispersion is one of the main pollution sources in the production environment. However, the transport process of industrial bulk materials is usually carried out outdoors, which further aggravates dust pollution due to the existence of transverse airflow. Dust pollution causes a series of problems to the environment and industry. For example, serious hazards to workers' health and dust explosions. Studies have shown that prolonged exposure to dust can lead to pneumoconiosis [1, 2]. Bulk materials such as coal powder, aluminum powder and cement occupy a considerable proportion of the industrial raw materials. During the transport of bulk materials a large amount of dust is generated, especially PM10 respirable particles which have a significant impact on human health [3]. Therefore,

the mechanisms of dust diffusion are great importance to research during the transport process of bulk materials.

Dust diffusion is essentially a matter of particle migration in the presence of induced airflow. Bagnold [4] was the first to investigate the mechanism of wind-driven particle motion. In recent years, several scholars have studied particle dispersion by means of field measurements, wind tunnel tests and numerical simulations. Roney and White [5] estimated PM10 emission rates for four different soils through wind tunnel tests. Kang and Guo [6] have conducted numerical simulations of wind and sand movement based on Computational Fluid Dynamics to reveal the dynamics of wind and sand movement and the discrete properties of particles at the individual particle level. The mechanisms of particle movement in the airflow include aerodynamics and aerosol mechanics [7, 8]. Sun studied the particle flow free and adherent fall processes by experiments and coupled CFD-DEM simulations, and it was found that the entrained airflow field is mainly influenced by larger particles [9–11]. Respirable dust particles prefer to remain suspended in the air and move with the airflow [12]. Patankar and Joseph [13] proposed a Eulerian–Lagrangian numerical simulation format for granular flows and simulated the spatial distribution

✉ Hongfa Sun  
sunhf1212@xtu.edu.cn

<sup>1</sup> College of Civil Engineering, Xiangtan University,  
Xiangtan 411105, Hunan, China

characteristics of particles in different airflow fields. Stone [14] used a coupled CFD-DPM phase approach to study the diffusion and sedimentation of particles in horizontal airflow, as well as suggesting that the coupled approach can provide effective predictions for simplified and reproducible processes. Witt [15] used CFD modelling to study airflow and dust lift-off around a bed of particles on a conveyor belt. Four turbulence models were analysed by Torno and the k-ε model was chosen to investigate the dust emissions of PM10 and PM50 on the conveyor belt [16]. Morla [17] simulated the diesel particulate matter generated during the movement of a transfer transport tipper and analysed the effect on the spatial concentration distribution of particle in different flow fields and at different locations. The spatial distribution of dust from self-propelled peanut combine harvesters under different operating conditions was evaluated using a CFD model by Xu [18].

In summary, current studies on dust initiation are mainly wind and sand initiation studies. Wind-blown sand initiation and dust diffusion are generally stationary for dust sources. However, the dust source is in a moving state during the transport of industrial bulk materials. For example, different bulk material transfer methods such as conveyors and trucks. There is a lack of research in the existing literature on dust sources in a moving state. Based on this, this study establishes the physical model of particle diffusion of mobile dust source under different working conditions and numerically simulates the mobile dust source based on the coupled CFD-DPM method. The results of the study provide a theoretical basis for dust fugitive control during the transportation of industrial bulk materials.

## 2 Numerical modeling and validation

### 2.1 Continuous phase equation

The temperature change is neglected during dust diffusion, so there is no need to solve the energy equation [1, 19]. In this study, it is simulated under turbulent regime. The environment around the mobile dust source is considered as a steady air flow, and the air bypasses the dust source ignoring its density variations. Hence the surrounding air is an incompressible fluid. The continuity equation and momentum equation are obtained by time-averaging the Navier–Stokes equation as:

$$\frac{\partial \rho}{\partial t} + \frac{\partial}{\partial x_i} (\rho u_i) = 0 \tag{1}$$

$$\frac{\partial}{\partial t} (\rho u_i) + \frac{\partial}{\partial x_j} (\rho u_i u_j) = -\frac{\partial P}{\partial x_i} + \frac{\partial}{\partial x_j} \left[ \mu \left( \frac{\partial u_i}{\partial x_j} + \frac{\partial u_j}{\partial x_i} - \frac{2}{3} \delta_{ij} \frac{\partial u_l}{\partial x_l} \right) \right] + \frac{\partial}{\partial x_j} (-\overline{\rho u'_i u'_j}) \tag{2}$$

where  $\rho$  is the air density,  $\text{kg/m}^3$ ;  $x_i$  and  $x_j$  are both coordinate components of the Cartesian coordinate system,  $i, j = 1, 2, 3$ ;  $u_i$  and  $u_j$  denote the velocity components in the  $x_i$  and  $x_j$  directions,  $\text{m/s}$ ;  $P$  denote the static pressure,  $\text{Pa}$ ;  $\delta_{ij}$  is the Kronecker delta;  $l$  denote the phase- $l$ .

A Reynolds stress term containing the pulsation value  $\overline{\rho u'_i u'_j}$  is introduced into the Eq. (2).

$$-\overline{\rho u'_i u'_j} = \mu_t \left( \frac{\partial u_i}{\partial x_j} + \frac{\partial u_j}{\partial x_i} \right) - \frac{2}{3} \rho k \delta_{ij} \tag{3}$$

$$\mu_t = \rho C_\mu \frac{k^2}{\epsilon} \tag{4}$$

The k-ε model proposed by Launder and Spalding, which is widely used in turbulence engineering, is adopted considering that dust diffusion is affected by turbulence [12, 19, 20]. Where,  $k$  is the turbulent kinetic energy and  $\epsilon$  denotes the dissipation rate of turbulent kinetic energy. The Realizable k-ε model is chosen in this study to better correct for vorticity and backflow. Higher confidence and accuracy in a wider range of flows [21]. The  $k$  equation and  $\epsilon$  equation are:

$$\frac{\partial}{\partial t} (\rho k) + \frac{\partial}{\partial x_i} (\rho k u_i) = \frac{\partial}{\partial x_i} \left[ \left( \mu + \frac{\mu_t}{\sigma_k} \right) \frac{\partial k}{\partial x_i} \right] + G_k + G_b - \rho \epsilon - Y_M + S_k \tag{5}$$

$$\begin{aligned} \frac{\partial}{\partial t} (\rho \epsilon) + \frac{\partial}{\partial x_j} (\rho \epsilon u_j) = & \frac{\partial}{\partial x_j} \left[ \left( \mu + \frac{\mu_t}{\sigma_\epsilon} \right) \frac{\partial \epsilon}{\partial x_j} \right] \\ & + \rho C_{1\epsilon} S_\epsilon - \rho C_{2\epsilon} \frac{\epsilon^2}{k + \sqrt{\nu \epsilon}} + C_{1\epsilon} \frac{\epsilon}{k} C_{3\epsilon} G_b + S_\epsilon \end{aligned} \tag{6}$$

$$C_1 = \max \left[ 0.43, \frac{\eta}{\eta + 5} \right] \tag{7}$$

where  $\mu$ ,  $\mu_t$  denote the laminar viscosity coefficient and turbulent viscosity coefficient, respectively,  $\text{Pa}\cdot\text{s}$ ;  $G_k$  denotes turbulent kinetic energy generated by laminar velocity gradient;  $G_b$  is the generation of turbulence kinetic energy due to buoyancy force;  $Y_M$  denotes the fluctuation due to excessive diffusion, in this study it is assumed that the gas is incompressible, therefore  $Y_M$  is 0;  $t$  denotes time;  $\sigma_\epsilon$  and  $\sigma_k$  are the Prandtl numbers corresponding to the turbulent kinetic energy  $k$  and the dissipation rate of turbulent kinetic energy  $\epsilon$ , respectively;  $C_{2\epsilon}$ ,  $C_{1\epsilon}$  and  $C_{3\epsilon}$  are empirical constants, where  $-\rho C_{2\epsilon} \frac{\epsilon^2}{k + \sqrt{\nu \epsilon}}$  is the dissipation term and  $C_{1\epsilon} \frac{\epsilon}{k} C_{3\epsilon} G_b$  is the buoyancy correction term. In Fluent, the default values of the parameters are as follows:  $\sigma_\epsilon = 1.2$ ,  $\sigma_k = 1.0$ ,  $C_2 = 1.9$ ,  $C_{1\epsilon} = 1.44$  and  $C_{3\epsilon} = 0.09$  [22, 23];  $\nu$  represents the velocity component of the fluid parallel to the direction of gravity;  $S_k$  and  $S_\epsilon$  are the defined the source term of turbulent kinetic energy,  $\eta = S_\epsilon^k$ ,  $S = \sqrt{2 S_{ij} S_{ij}}$ ,  $S_{ij} = \frac{1}{2} \left( \frac{\partial u_i}{\partial x_j} + \frac{\partial u_j}{\partial x_i} \right)$ ,  $S_{ij}$  is strain rate tensor, which corresponds to the symmetric part of the gradient of velocity tensor.

Equations (1)–(7) is a complete description of the flow field around mobile dust sources and the system of equations is closed.

This section corresponds to the viscous model part of Fluent, which describes the continuous phase turbulence model in the fluid domain of the physical model established in this paper.

### 2.2 Discrete phase equation

In the discrete particle trajectory model [1], according to Newton’s second law, the equilibrium equation for the force on the particle is:

$$m_p \frac{dv}{dt} = F_d + F_g + F_f + F_x \tag{8}$$

where,  $m_p$  is dust mass, mg;  $v$  is dust velocity, m/s;  $m_p \frac{dv}{dt}$  denote inertia force, N;  $F_d$  is the drag force,  $F_f$  is buoyancy,  $F_g$  is gravity;  $F_x$  is the other forces on the particle, including pressure gradient force, Saffman force, virtual mass force, etc.

This study is conducted at a constant temperature field and does not activate the energy equation, so thermophoretic forces and Brownian force are not considered [24]. So the other additional forces  $F_x$  on the particle are considered only Saffman force, pressure gradient force and virtual mass force.

Taking into consideration the effects of drag force, gravity, buoyancy and Saffman forces, the particle equations of motion according to Eq. (8) is expressed as follows [22, 24]:

$$m_p \frac{dv}{dt} = m_p \frac{(v' - v)}{\tau_r} + m_p \frac{g(\rho_p - \rho)}{\rho_p} + F_x \tag{9}$$

$$\tau_r = \frac{\rho_p d_p^2}{18\mu} \frac{24}{C_D Re} \tag{10}$$

where  $\rho$  and  $\rho_p$  are the densities of fluid and particles, respectively, kg/m<sup>3</sup>;  $\tau_r$  is the particle relaxation time;  $d_p$  is the particle diameter, m; and  $C_D$  is the drag coefficient.

In Eq. (9), the first term represents the drag force, the second term represents gravity and buoyancy. Where the drag force is generated by the relative motion occurring between the particles and the fluid.

For sub-micron particles, a form of Stokes’ drag law more suitable for small particles is available. In this case,  $F_d$  is defined as:

$$F_d = m_p \frac{(v' - v)}{\tau_r} = m_p \frac{18\mu}{d_p^2 \rho_p C_c} (v' - v) \tag{11}$$

where,  $C_c$  is the Cunningham correction factor  $C_c = 1 + \frac{2\lambda}{d_p} \left( 1.257 + 0.4e^{-(1.1d_p/2\lambda)} \right)$ , and  $\lambda$  is the mean free path of the molecule, 10<sup>-8</sup> m. The Cunningham correction improves drag predictions for the slip flow or transitional regime between the continuum and free-molecular flow regimes.

This section corresponds to the Discrete Phase Model part of Fluent, which describes the diffusion of discrete-phase particles in reaction to air erosion [25].

### 2.3 Physical model and boundary conditions

In this paper, dust initiation from a mobile dust source is studied by establishing a three-dimensional rectangular fluid control domain [26]. The physical model was built using SpaceClaim 2020 R2 software (A 3D modeling software) [27, 28]. As shown in Fig. 1, the total length of the fluid field is 2500 mm, the width is 1500 mm and the height is 800 mm. Based on the actual industrial bulk material transfer and conveying process, the dust source has a length of 1000 mm, a width of 500 mm and a height of 375 mm above the ground. The distance from the dust source to the inlet is 500 mm and to the outlet is 1000 mm. Dust particles are adhered to the surface of the mobile dust source (red shaded surface), and set the injection velocity  $v_i$  of the particles (the magnitude and direction are consistent with the mobile surface). The particles diffused from the red shaded surface by the erosion of the free flow (The diffusion manner shown in the inserted figure in Fig. 1). The main study is the diffusion of particles above and behind the dust source. The boundary conditions are shown in Table 1.

In the fluid control domain, the left inlet is set to “velocity-inlet”, the right outlet is set to “pressure-outlet”, and the rest of the wall is set to “no-slip” boundary condition. In order to objectively reflect the dust production of mobile dust sources, the dust source (red shaded surface in Fig. 1) is set as the mobile dust source particle release area. The injection type is “Surface”, the wall condition is set to “Moving wall” (The “Dust source mobile velocity” is changed by changing the velocity of the “Moving wall”, like a conveyor belt.), and the discrete phase model condition is set to “Reflect”. Before the particles are affected by the air flow, the “Particle injection velocity” is set to be the same as the “Dust source mobile velocity”, i.e., the particles are generated and then moved together with the dust source (no relative motion). Except for the mobile dust source other boundary discrete phase model conditions are set to “escape”, in order to avoid the impact of particles bouncing at the boundary on the particles in the study area. Considering the simplification of the model, the shape of the dust particles is considered as a smooth sphere, so the rotation of the particles and the lifting force

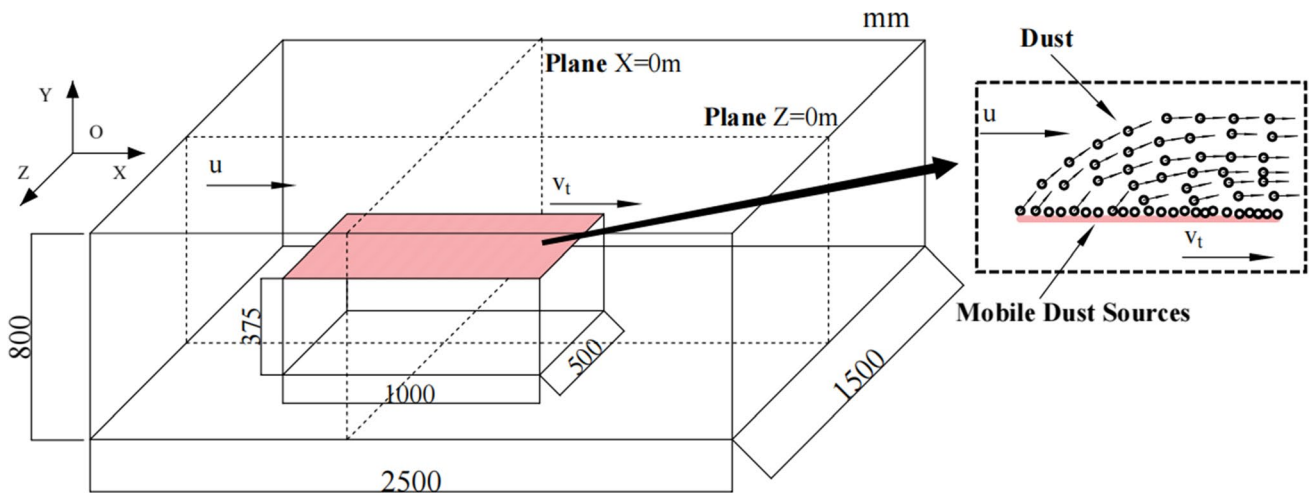


**Fig. 1** Physical model and diffusion mechanism ( $u$  denotes wind velocity and  $v_t$  indicates the velocity of mobile dust source in the figure)

**Table 1** Boundary conditions

Conditions	Dust source mobile velocity ( $v_t$ , m/s)	Diameter ( $d_p$ , $\mu\text{m}$ )	Wind velocity ( $u$ , m/s)	Variables
1, 2, 3, 4, 5, 6, 7	0, 2, 4, 6, -2, -4, -6	1–10	7.5 (moderate breeze)	Dust source mobile velocity ( $v_t$ , m/s)
8, 3, 9, 10, 11	4	1, 2.5, 5, 7.5, 10	7.5 (moderate breeze)	Particle diameter ( $d_p$ , $\mu\text{m}$ )
12, 13, 3, 14	4	1–10	0.5 (calm), 3 (entle breeze), 7.5 (moderate breeze), 10 (fresh breeze)	Wind velocity ( $u$ , m/s)

**Table 2** Object phase parameters

Parameter	Value
Air density ( $\text{kg}/\text{m}^3$ )	1.225
Air viscosity ( $\text{kg}\cdot\text{s}/\text{m}$ )	$1.7894 \times 10^{-5}$
Dust density ( $\text{kg}/\text{m}^3$ )	1400

caused by the rotation process are neglected. Taking coal powder as an example, the actual production process of coal powder diameter is mostly Rosin–Rammmler distribution [29]. The object phase parameters are set as shown in Table 2.

For the Euler–Lagrange model, the Semi-Implicit Method for Pressure Linked equations (SIMPLE) algorithm is used to couple the gas pressure and velocity [25]. The SIMPLE algorithm is a pressure amendment method that obtains the pressure field by “guessing first and then amending”, and solves the discretized Eq. (2). The pressure, momentum, turbulent energy and turbulent dissipation rate in the differential format are simulated using the Second Order Upwind. The Second Order Upwind Format is based on the backward difference scheme for the discretization of the spatial terms (second order partial derivatives) from Eqs. (2), (5), and (6).

**Table 3** DPM parameters and settings

Parameter	Value
Injection type	Surface
Particle type	Inert
Material	Coal
Diameter distribution	Rosin–Rammmler
Min. diameter(m)	$1 \times 10^{-6}$
Max. diameter(m)	$1 \times 10^{-5}$
Mean diameter(m)	$4.45 \times 10^{-6}$
Spread parameter	3.5
Total flow rate(kg/s)	$1 \times 10^{-5}$
Discrete random walk model	on

The discrete phase model (DPM) parameters are set (including particulate matter parameters and modelling methods) as shown in Table 3. “Surface” means that the injection source is a surface domain; “Inert” means that the inertial particles obey Eqs. (8) and (9), i.e., force equilibrium; “Discrete Random Walk(DRW) Model” simulates the interaction of particles with fluid turbulent eddies as well as being able to predict particle dispersion due to turbulence in the fluid phase. The DRW model includes the effect of instantaneous turbulent velocity fluctuations on the particle

trajectories through the use of stochastic methods, i.e., predicting the trajectories of the particles using the fluid phase mean velocity in Eq. (9).

In the calculation of the particle motion trajectory, by the coupled CFD-DPM method (using a two-way coupling of continuous-phase airflow and discrete-phase particles), not only the effect of air on particles but also the effect of particles on the flow field is taken into account. The effect of the discrete phase on the continuous phase is considered as an additional source term in Eqs. (1) to (7).

### 2.4 Model validation

The particle vertical velocity is used as an important parameter for dust lifting-off from the dust source. The current positions and velocities of all particles existing in the computational domain are exported in Fluent’s Particle Tracks panel, and the upward velocities of all particles on the dust source surface are obtained by filtering. This study was conducted by comparing the particle vertical velocities in the literature [30]. As shown in Fig. 2, the distributions of particle vertical velocities under three working conditions when the dust source is static and the dust source is mobile at 6 m/s and – 6 m/s. According to the curve fitting of the three sets of simulated data respectively, it can be observed that the vertical velocities of the three working conditions follow exponential distribution and the correlation coefficients  $R^2$  are greater than 0.99, which indicates that the regression effect is good.

In order to study the lift-off of dust particles from the surface of the dust source, the dusting velocity is introduced to determine the movement of the particles. Particle dusting velocity refers to the velocity component of the particle

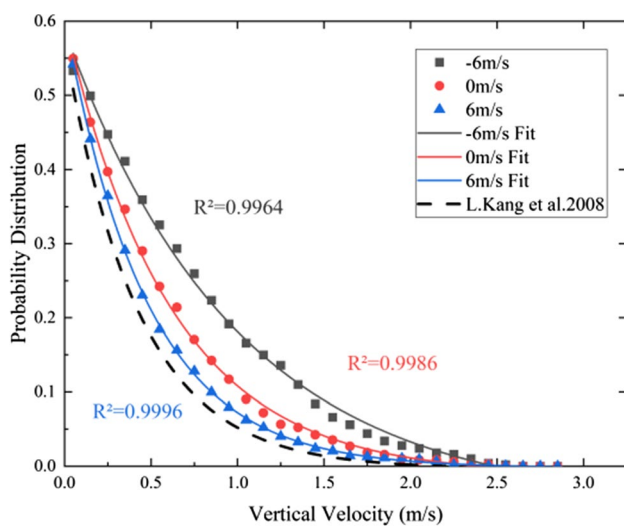


Fig. 2 Probability distribution of the vertical upward velocity of the particle

velocity vertically upward, which is larger than 0 for dusting particles. The formula for calculating the mean dust velocity of particles is:

$$\bar{v}_y^+ = \sum_{k=0}^{N-1} \eta_k v_{yk}^+ \tag{12}$$

$$\eta_k = \frac{1}{N} \tag{13}$$

where,  $v_{yk}^+$  denotes the vertical velocity component of dusting particle  $k$ , m/s;  $\eta_k$  is the weighting factor;  $N$  is the sample number of dust-raising particles.

As shown in Fig. 3, the relative velocities ( $u-v_t$ ) of the free airflow and the moving dust source are found to be proportional to the mean vertical upward velocity of the particles according to the variation rule.

In addition, the dust flux is used as an important indicator of wind and sand initiation. By analyzing the particle vertical velocity distribution pattern, the mean value of vertical velocity is used as the initial condition for particle dust initiation.

The dust flux is the mass of dust passing through a unit area from down to up in a horizontal plane per unit time, and its calculation formula is:

$$q_d = \int C_p \bar{v}_y^+ dA = \sum_{w=1}^n C_{pw} \bar{v}_{yw}^+ A_w \tag{14}$$

where,  $q_d$  is dust flux, kg/s;  $C_p$  denote particle mass concentration, kg/m<sup>3</sup>;  $A$  is the horizontal surface area, m<sup>2</sup>.

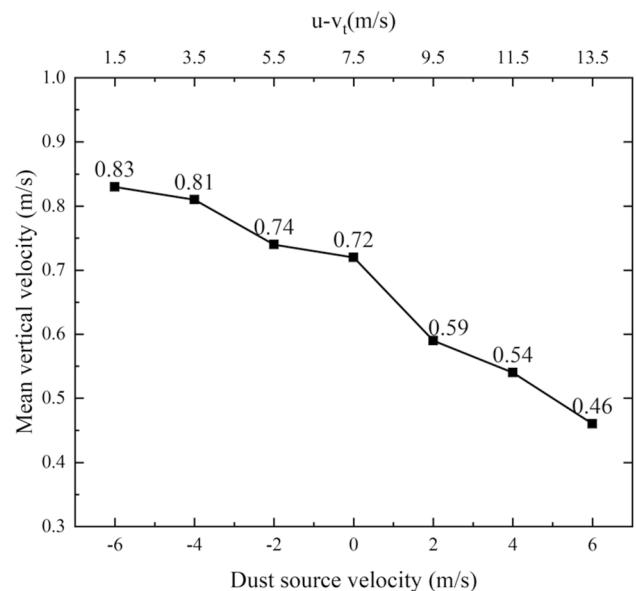


Fig. 3 Mean vertical upward velocity of particles with different dust source mobile velocities and different relative velocities

The reason for using mass fluxes higher than 0.005 m for the analysis in this study is that mass fluxes near the bed are related to differences in particle transport patterns. Particle collisions lead to large uncertainties in the trajectory, and creeping and saltating particles may introduce additional near-bed mass fluxes. In this paper, we compare the total mass flux with height for sand particles at a simulated shear velocity of 0.63 m/s by Kang [30] and for mixed particle size particles measured at a wind speed of 12 m/s by Tan [31]. The calculated vertical distribution of particle mass fluxes and the fitted curves are shown in Fig. 4. The fitted curve can be described by the following function:

$$y = A \exp(-x/b) - y_0 \tag{15}$$

where the value of A is 219; the value of b is  $1.75e^{-5}$ ; and the value of  $y_0$  is  $-17.8$ .

It can be found that the mass flux decreases exponentially with height, and this pattern of distribution is consistent with many scholarly studies. The experiment of Dong [32] showed that the dust mass flux decreased exponentially with height. In field measurements and numerical simulations by Namikas [33] found that the vertical distribution of mass fluxes followed an exponential distribution. Xiao [34]. showed an exponential decrease of sand mass flux with height by numerical simulation.

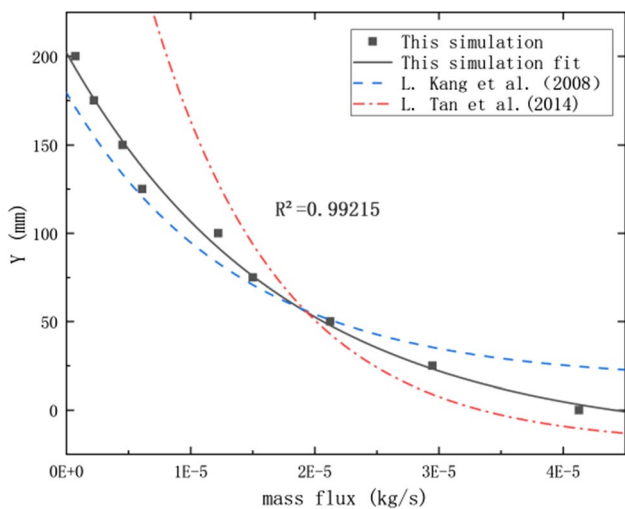


Fig. 4 Vertical distribution of particle mass flux

### 3 Results and discussion

#### 3.1 Flow field and contour analysis

##### 3.1.1 Flow field analysis

The results analysed in this paper are all based on simulations to reach a steady-state-like regime. When the inlet wind velocity is 7.5 m/s, the dust source moves at a velocity of 4 m/s. The flow field nearby the dusting surface is shown in Fig. 5. The elevated structure of the dust lifting surface reduces the cross-sectional area of the airflow path and the maximum airflow velocity above the dust lifting surface is 12.5 m/s, which is 1.6 times the inlet velocity. At the same time, backflows and vortices occur above, sideways and behind the elevated structure with a certain entrainment effect. The existence of the vortex makes the flow vertical to the dusting surface direction, which is helpful for the movement of particles in the vertical direction, so the dusting effect is more obvious [35]. The vorticity of the vortex increases with the increase of the inlet wind velocity, and the disorder of particles in the vortex region is positively correlated with the vorticity.

##### 3.1.2 Particle diffusion position in the middle section

As shown in Fig. 6, in order to quantitatively analyze the concentration distribution patterns of PM10 dust in the flow field, nine straight lines are drawn in the  $Z=0$  plane, which were located at 25 mm, 50 mm, 75 mm, 100 mm, 125 mm, 150 mm, 175 mm, 200 mm and 225 mm above the dust initiation surface and indicated the line graphs of the concentration distribution at each height. The maximum dust concentration on a straight line at a height of 25 mm is  $1.05e^{-4} \text{ kg/m}^3$  and is located close to the front of the mobile dust source. A significant decrease in dust concentration occurs at the end of the mobile dust source. Comparing the particle concentrations at different heights, the dust concentration decreases with increasing height and the peak of each concentration gets closer to the  $X=0$  position (i.e. the middle of the mobile dust source) with increasing height.

In this paper, the diffusion contour curves for dust are contours of mass concentration (i.e., connecting the points of each equal particle mass concentration.). The diffusion contour diagram allows to visualize the range of dust mass concentrations at different spatial locations. In order to make the mass concentrations at the different locations selected obvious, four different mass concentration contour curves of  $3e^{-5} \text{ kg/m}^3$ ,  $1e^{-5} \text{ kg/m}^3$ ,  $5e^{-6} \text{ kg/m}^3$  and  $1e^{-6} \text{ kg/m}^3$  are selected in this paper. As shown in Fig. 7,

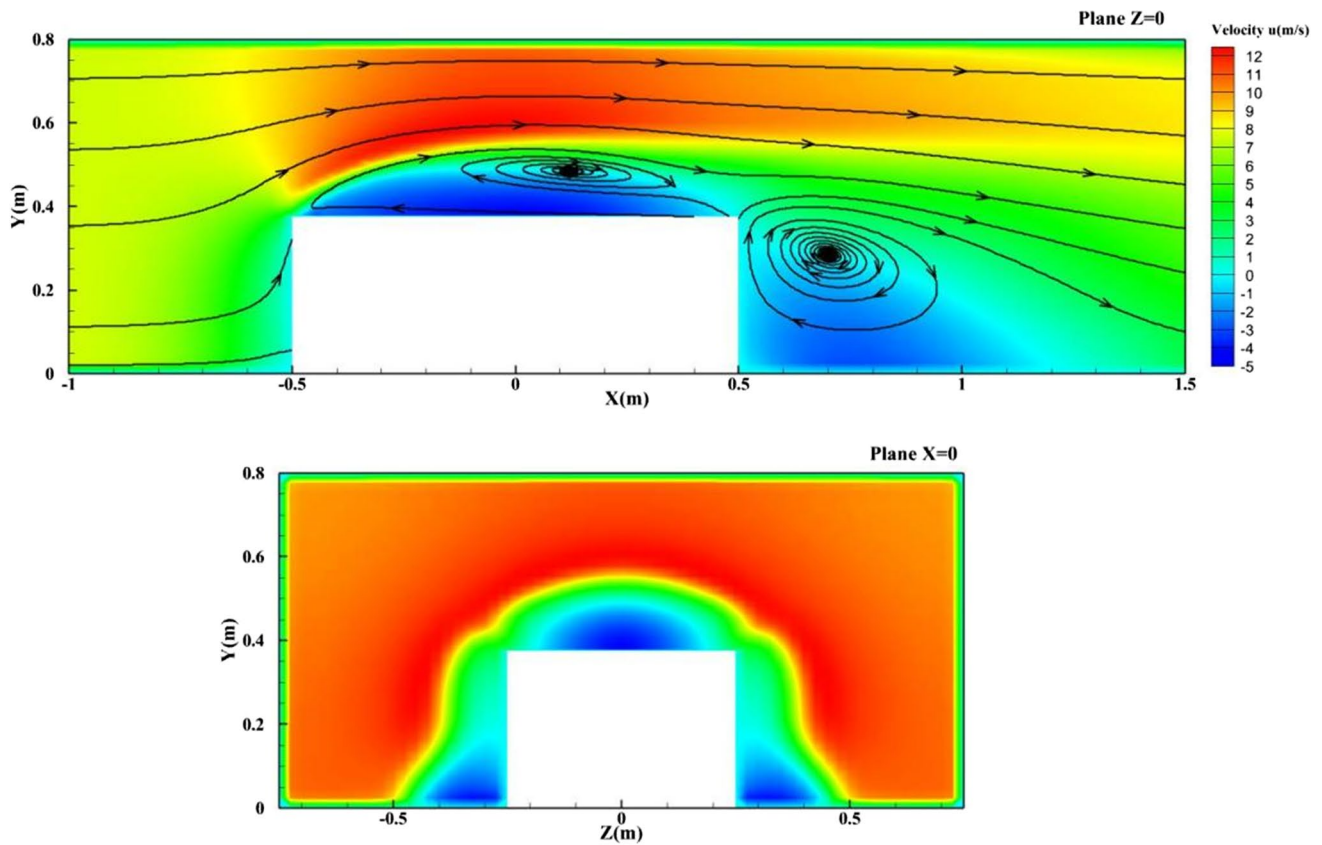
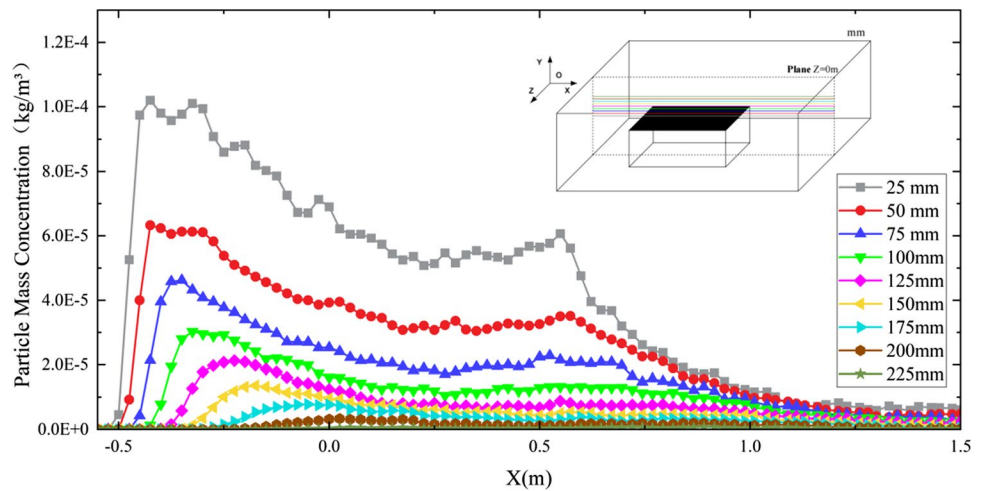


Fig. 5 Flow field distribution and streamlines

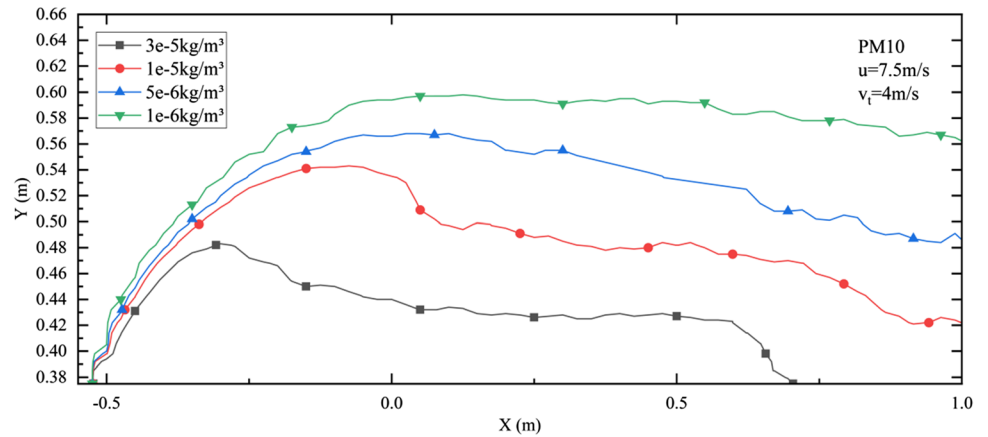
Fig. 6 Distribution of PM10 dust concentration at different heights



the diffusion contour diagram representing the four concentrations of PM10 particles in the  $Z=0$  plane. The study area location in the figure is above the mobile dust source, the horizontal location includes the mobile dust source and the 0.5 m range behind it. The trend of dust particle diffusion is observed and analyzed in this range. The peak diffusion height of the contour line of  $3e^{-5}$   $\text{kg}/\text{m}^3$  is 0.1 m,

which is 0.07 m on average. The diffusion range is in the vicinity of the mobile dust source, and the deposition is obvious at 0.2 m at the rear end of the dust source. The peak contour diffusion height of  $1e^{-5}$   $\text{kg}/\text{m}^3$  is 0.16 m and the average is 0.12 m. The average diffusion height of the contour line for  $5e^{-6}$   $\text{kg}/\text{m}^3$  is about 1.9 m. The  $1e^{-6}$   $\text{kg}/\text{m}^3$  contour line average diffusion height is about 0.22 m.

**Fig. 7** Diffusion contours of different concentrations in the Z=0 plane



Among them, the height peaks of the diffusion contour line for  $3e^{-5} \text{ kg/m}^3$  and  $1e^{-5} \text{ kg/m}^3$  concentrations are more obvious. However, the height of the diffusion contour line for  $3e^{-5} \text{ kg/m}^3$ ,  $1e^{-5} \text{ kg/m}^3$  and  $5e^{-6} \text{ kg/m}^3$  concentrations tends to decrease with the horizontal direction. The height of the diffusion contour line for the concentration of  $1e^{-6} \text{ kg/m}^3$  remains stable with the horizontal direction. According to the results in Fig. 7, there are larger mass concentrations at the lower positions.

In summary, the dust concentration decreases with increasing height, and the peak concentration at each horizontal height becomes more and more backward with increasing height.

### 3.1.3 Regional division of different particle diffusion patterns

The diffusion contour diagram and airflow field analysis for different concentrations in the Z=0 plane can be roughly divided into three different dust particle diffusion region A, B and C. It can be further explained that each region has a

direct or indirect effect on the dust diffusion [36]. As shown in Fig. 8, different regions of the dust diffusion pattern can be identified from the figure:

Region A: The boundary layer area close to the moving dust source. In this region the dust particles are affected by the shear airflow from the dust source plane.

Region B: The air flow forms a vortex region above the dust source. The dust gains further velocity in the vertical direction by the action of the vortex and is partially suspended or deposited.

Region C: Horizontal airflow area. The dust particles follow the airflow at a certain height and continue to spread in the horizontal direction.

## 3.2 Particle concentration distribution

### 3.2.1 Effect of the wind velocity on particle concentration distribution

The force on the particles under the action of the airflow can be seen according to Eq. (8), by which the force gains

**Fig. 8** Division figure

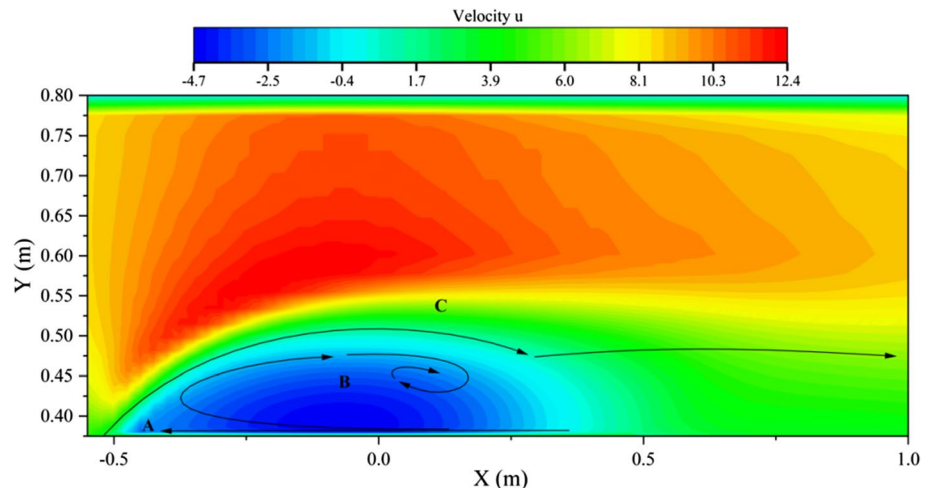
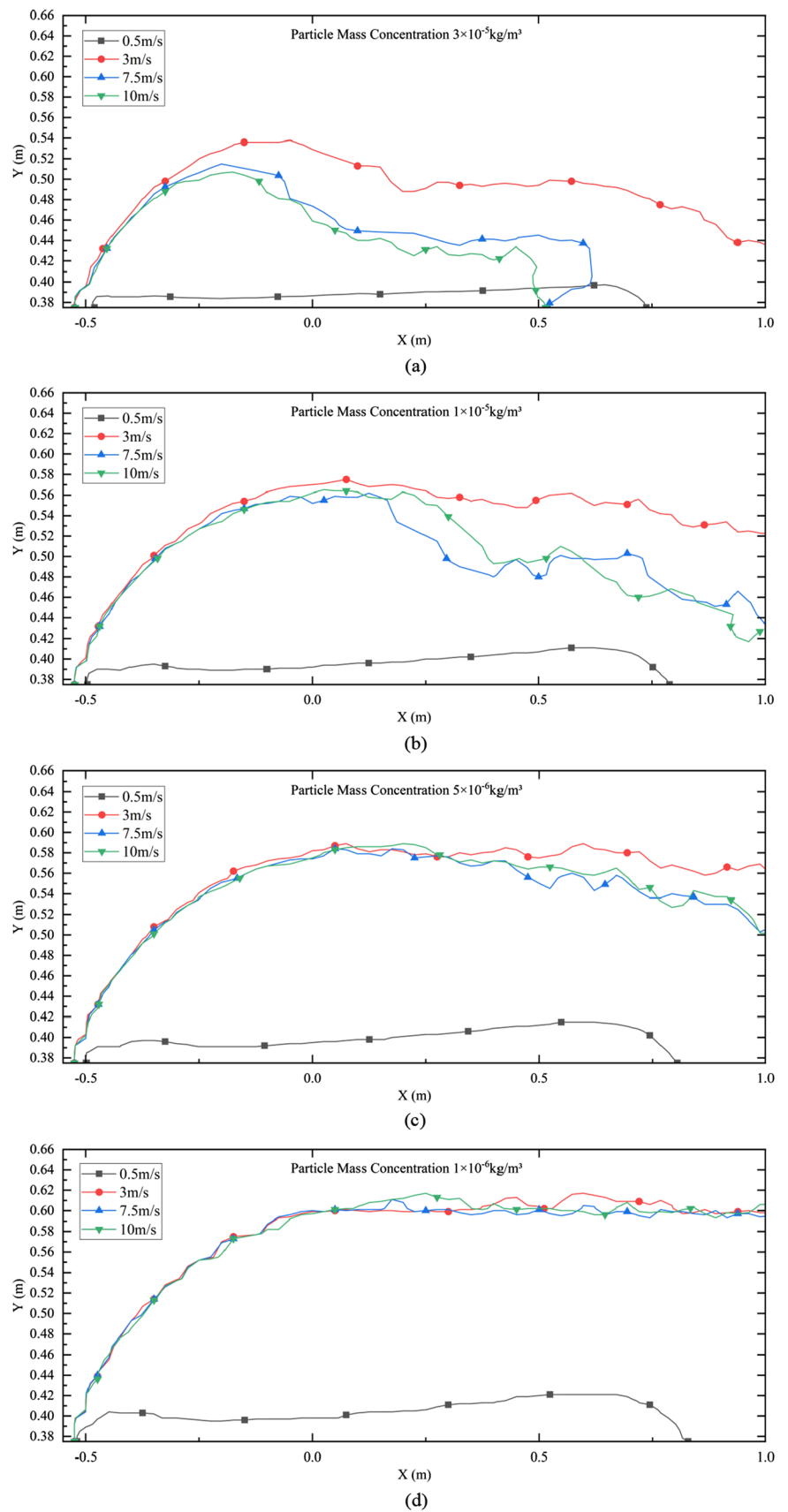




**Fig. 9** Contour diagram of particle diffusion at different wind velocities (PM10,  $v_t = 4$  m/s)



an upward velocity and diffuses. As shown in Fig. 9, the diffusion contours of different concentrations at different wind velocities are shown. The wind velocities of 0.5 m/s, 3.0 m/s, 7.5 m/s and 10 m/s are selected to study the effect on the dust initiation of mobile dust sources. Under calm conditions, the diffusion contours of each concentration do little change, all diffusing in the vicinity of the mobile dust source, whose maximum dust initiation height is around 0.1 m. The comparison shows that the diffusion contours of different concentrations are similar at wind velocity 7.5 m/s and 10 m/s conditions. In Fig. 9a, b, it is found that the diffusion contour curves are significantly different from all other wind conditions at wind velocity of 3 m/s. Higher concentrations of particles spread higher, farther and wider. At lower concentrations, the diffusion contour curves for the three wind velocity conditions tend to be consistent.

It can be seen the following rules by comparing the four different wind velocities. Under the calm condition, the dust is caused only by the airflow turbulence and particle collision caused by the mobile dust source, the diffusion height is lower and the range is smaller, which is not conducive to dust diffusion. In the gentle breeze conditions, the higher concentration of diffusion height and distance is greater than and moderate breeze and fresh breeze, which is most helpful for dust diffusion. The dust concentration diffusion trend is basically similar in the moderate breeze and fresh breeze conditions, without major differences. The height of the vortex region (Region B) is 0.143 m, 0.126 m and 0.12 m when the wind velocity is 3 m/s, 7.5 m/s and 10 m/s, respectively, which shows that the diffusion of higher concentration particles is positively correlated with the height of Region B.

### 3.2.2 Effect of the dust source mobile velocity on particle concentration distribution

As shown in Fig. 10, the different concentration diffusion contours corresponding to different dust source mobile velocity conditions are represented. As shown in Fig. 10a, in the higher concentration area close to the mobile dust source, the effect of different dust source velocity on dust diffusion is significant and distinct. When the dust source is stationary, the dust initiation height of the contour curve is significantly lower than for mobile dust sources. As the height from the mobile dust source increases and the concentration decreases, the effect of different dust sources mobile velocity on dust diffusion is little, which gradually tends to be consistent with the diffusion contour curve of different conditions. By comparing the effect of different dust sources velocity on particle concentration diffusion, it can be seen that different dust sources velocity has a greater disturbance on the flow field (Region A, B) close to the dusting surface. Mobile dust sources with high concentrations have higher dusting heights than stationary dust sources.

Little disturbance to the flow field away from the dusting surface and no effect on the flow field above the vortex region (Region C).

### 3.2.3 Effect of the particle diameter on particle concentration distribution

As shown in Fig. 11, the diffusion contours of different concentrations at different particle diameters are shown. Particle diameter less than or equal to 10 μm dust belongs to the micro-dust, in the air to do equal velocity deposition movement. It can be suspended in the air for a long time and has a long residence time when it is affected by airflow [37]. However, in the 0.15 m vertical range above the dust source is in the vortex caused by the return flow, the higher concentration of dust will be deposited significantly in this area. The dust above the vortex is reduced by the influence of the airflow in the vertical direction will spread in the horizontal direction with the airflow. The 7.5 μm curves in Fig. 11a–d have slightly higher average dust heights for the same dust concentration than for other particle diameters. The PM10 multi-particle diameter condition curve is basically consistent with the other single diameter condition curves except for 7.5 μm. In summary, the overall change in the diffusion contour of single and multi-grain dusts in the range of 1–10 μm is small, and the diffusion contour of 7.5 μm dust is a little higher than that of dusts of other grain diameters.

In summary, the analyses in Sects. 3.3.1–3.3.3 show that the conditions are consistent with the results in Figs. 8, 9: (1) Larger mass concentrations at lower locations. (2) Dust concentration decreases with increasing height.

## 3.3 Dust initiation rate

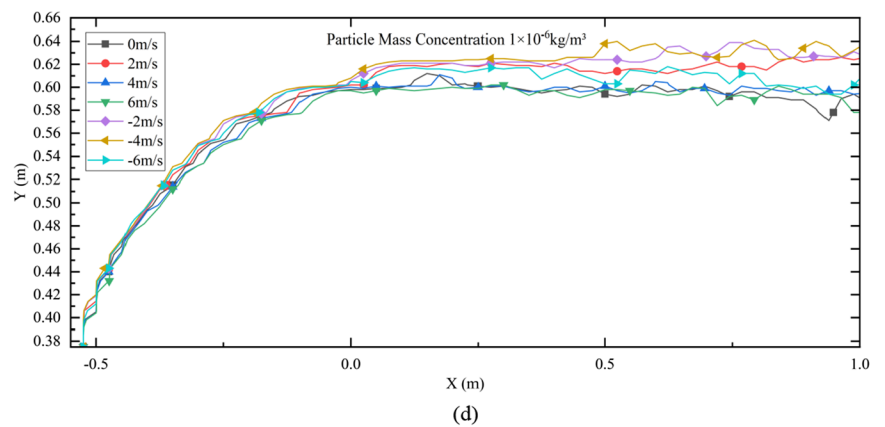
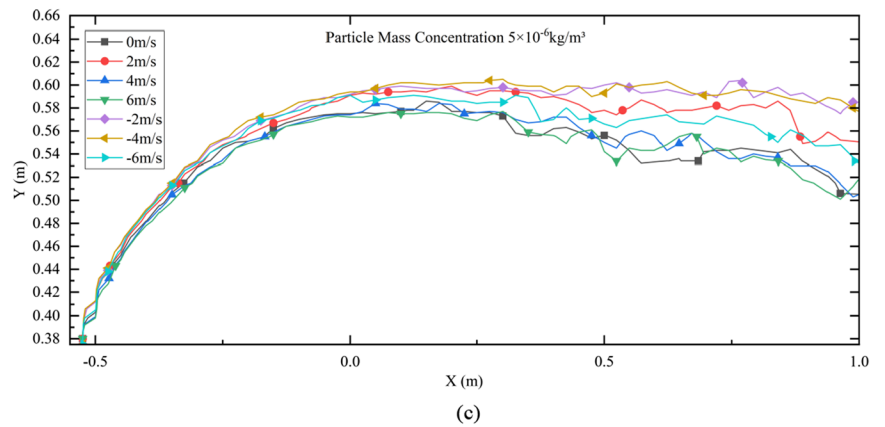
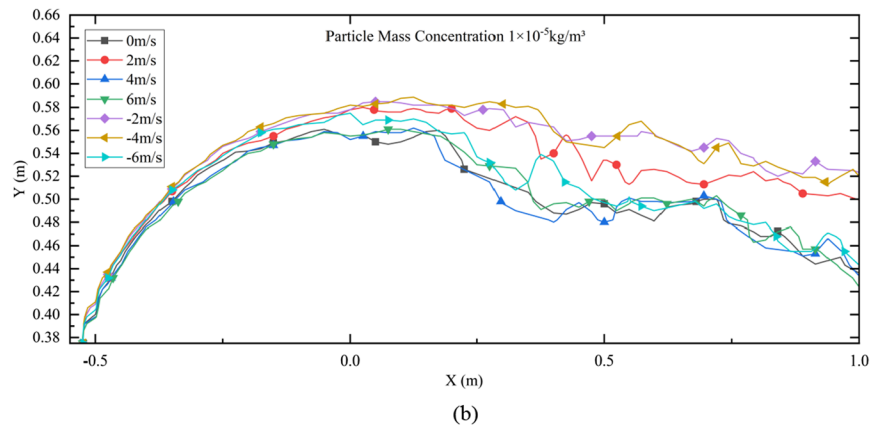
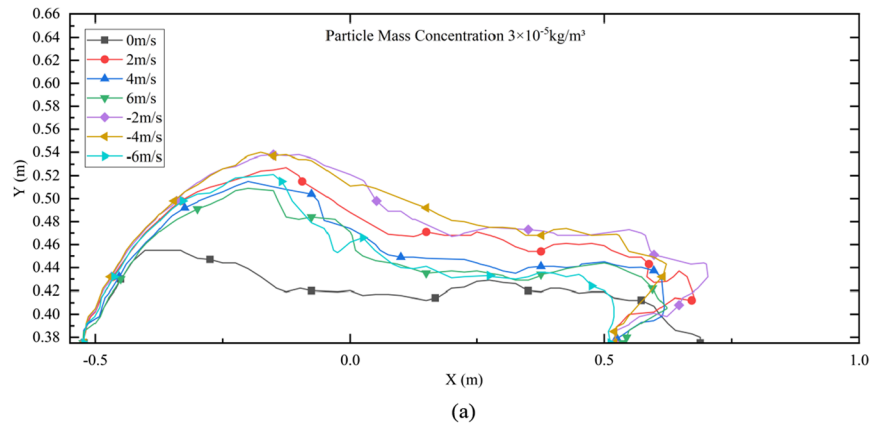
In this paper, the intensity of dust initiation per unit time on a certain horizontal surface is evaluated by defining the dust initiation rate.

The formula for calculating the dust initiation rate is:

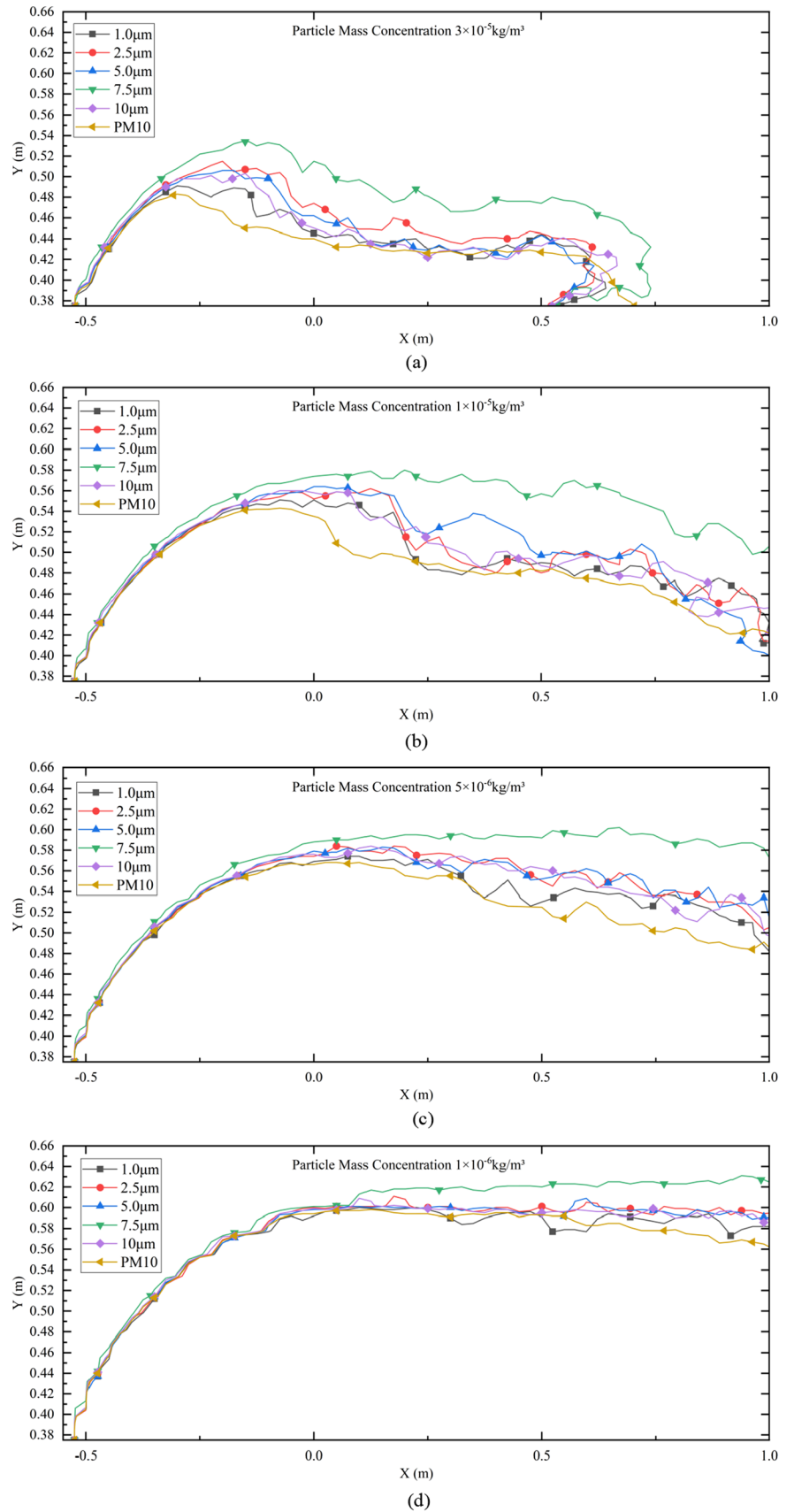
$$R_d = \frac{\text{Dusting mass flux through the horizontal plane}}{\text{Mass deposition load below the horizontal plane}} = \frac{q_d}{M} (1/s) \quad (16)$$

The variation of the dust initiation rate under different conditions is observed by three horizontal surfaces of different heights. The dust initiation rate of the mobile dust source from the dust surface to the airflow is studied at 0 mm (distance from dust surface), which expresses the overall dust initiation intensity of the mobile dust source. The study of the dust initiation rate at 50 mm and 100 mm above the dust surface were to understand the variation of the dust initiation intensity in the vertical direction for different conditions.

**Fig. 10** Contour diagram of particle diffusion with different dust source mobile velocity (PM10,  $u = 7.5$  m/s)



**Fig. 11** Diffusion contours of particles with different particle diameter ( $u = 7.5$  m/s,  $v_i = 4$  m/s)



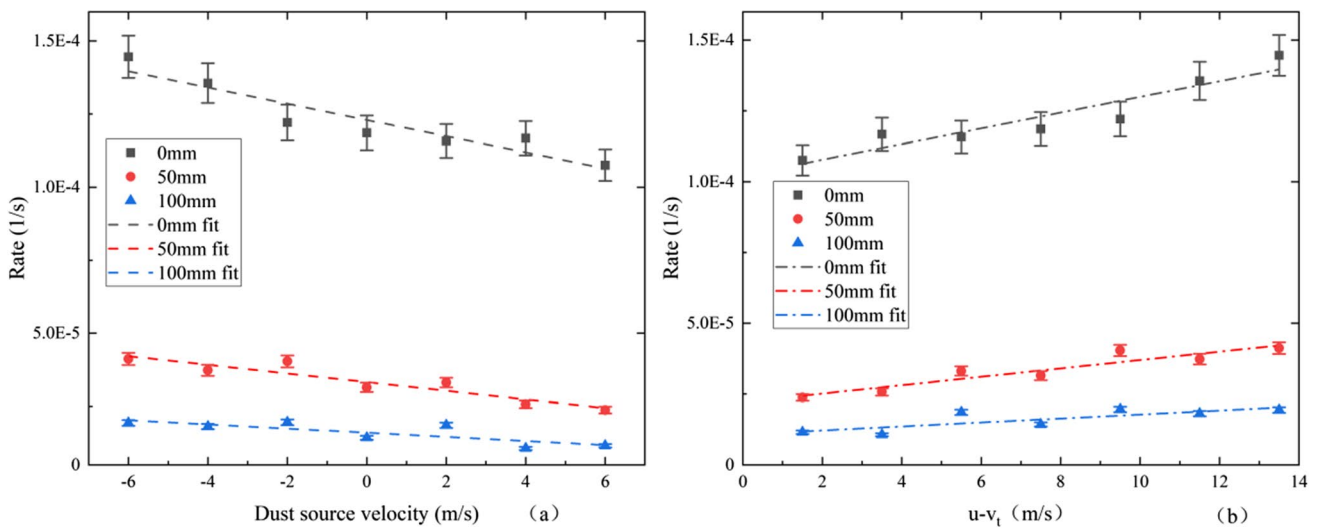


Fig. 12 Dust initiation rates for different dust sources mobile velocities and different relative velocities at different heights

### 3.3.1 Effect of dust source mobile velocity on dust initiation rate

As shown in Fig. 12, (a) shows the variation of dust initiation rate with different dust source mobility velocities at moderate breeze conditions. (b) is the variation of the dust initiation rate with the relative velocity magnitude of the airflow and the mobile dust source. When the dust source mobile direction is opposite to the airflow direction, the dust initiation rate increases with the wind velocity. When the dust source mobile direction is the same as the airflow direction, the dust initiation rate fluctuates with the increase of wind speed, but the overall trend decreases. For relative velocity, the dust initiation rate shows an overall increasing trend with increasing relative velocity. The trend of dust initiation rate decreases with the increase of height. The fluctuation of the values also decreases with the increase of height.

### 3.3.2 Effect of wind velocity on dust initiation rate

Figure 13 shows the variation of the dust initiation rate of a mobile dust source at different wind velocities. When the wind velocity increases, the dust initiation rate also increases. Compared with other conditions, the variation of wind velocity has the greatest effect on the dust initiation rate of the mobile dust source.

### 3.3.3 Effect of particle diameter on dust initiation rate

As shown in Fig. 14 is the variation of the dust initiation rate for different single particle diameter mobile dust sources. The dust initiation rate close to the dust source surface increases with particle diameter and then

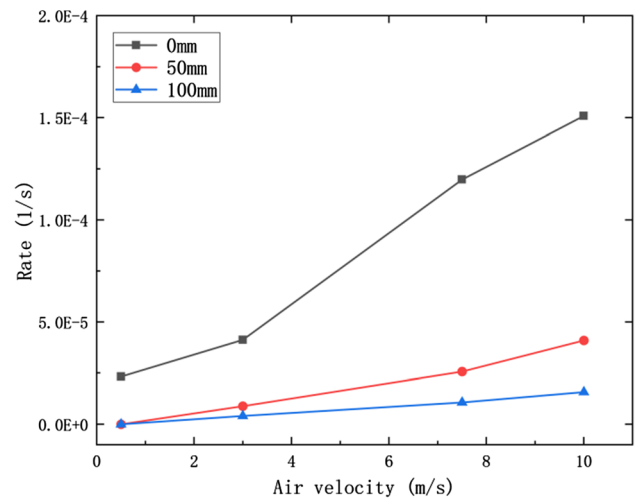
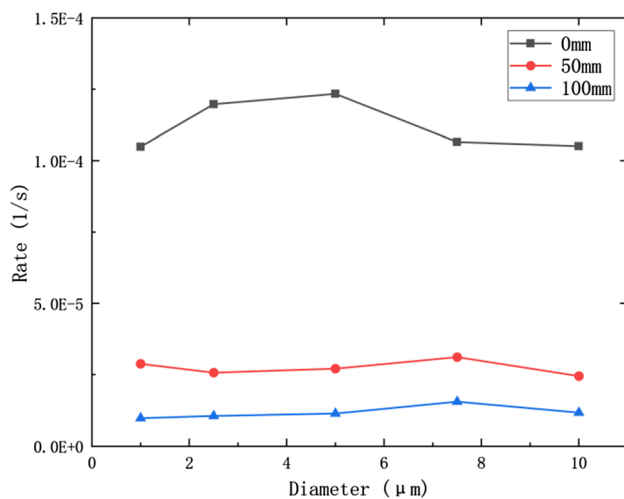


Fig. 13 Dust initiation rate at different heights and wind velocities

decreases. The maximum is reached at 5 μm. However, the overall effect of different particle diameters on the dust initiation rate changes little in the PM10 range. Essentially no effect at 50 mm and 100 mm height.

## 4 Conclusion

In this paper, the spatial distribution patterns of dust diffusion and dust concentration of mobile dust sources at different working conditions are studied to obtain conclusions as follows:



**Fig. 14** Dust initiation rates for different particle diameters at different heights

1. When in moderate breeze conditions, the flow field vortex intensity is smaller and the streamline is semi-annular. As the wind velocity increases, the streamline develops into an annular shape, and the intensity of the flow field vortex increases.
2. From the spatial distribution pattern of dust concentration, the dust concentration decreases with increasing height at the same working condition. Dust concentration of  $3e^{-5}$  kg/m<sup>3</sup> contour line average diffusion height of about 0.07 m, dust concentration reduced to  $1e^{-6}$  kg/m<sup>3</sup> contour line average diffusion height of about 0.22 m; The diffusion range is the smallest at a wind speed of 0.5m/s, and the maximum diffusion height of  $1e^{-6}$  kg/m<sup>3</sup> contour line is only 0.04 m. The diffusion range of the high concentration area decreases when the wind velocity is 7.5 m/s and 10 m/s. The average diffusion height of  $3e^{-5}$  kg/m<sup>3</sup> contour line is about 0.07 m, and the diffusion height is different from 0.05 m at the wind velocity of 3 m/s. Little change is shown in the low concentration range. The average diffusion height of  $3e^{-5}$  kg/m<sup>3</sup> contour line is about 0.05 m when stationary, and the average height of this contour line fluctuates from 0.08 to 0.12 m when mobile. 0.07 m is the maximum difference between the mobile velocity of  $-4$ m/s and stationary. When the particle diameter taken in this study is less than or equal to 10 μm, there is almost no effect on the dust diffusion and the spatial distribution of the concentration with the particle size as a variable.
3. From the results of the dust initiation rate, the most influential factor is the wind velocity. When the wind velocity is 0.5 m/s, the dust initiation rate is only  $2.5 \times 10^{-5}$  s<sup>-1</sup>. When the wind velocity reaches 10 m/s, the dust initiation rate is  $1.5 \times 10^{-4}$  s<sup>-1</sup>. The dust initiation rate grows with increasing wind velocity, and the variation range is

close to an order of magnitude. When the relative velocity of the mobile dust source and the airflow is 1.5 m/s, the dust initiation rate is  $1.1 \times 10^{-4}$  s<sup>-1</sup>. When the relative velocity increases to 13.5 m/s, the dust initiation rate is  $1.45 \times 10^{-4}$  s<sup>-1</sup>. The dust initiation rate tends to increase in general with the increase of relative velocity, with certain fluctuations and a variation range of less than  $5 \times 10^{-5}$  s<sup>-1</sup>. The overall effect of particle diameter on the dust initiation rate varied little, fluctuating only in the range of  $1 \times 10^{-4}$  s<sup>-1</sup> to  $1.25 \times 10^{-4}$  s<sup>-1</sup>.

**Acknowledgements** This work was supported by the Natural Science Foundation Youth Program of Hunan Province, China (Grant No. 2022JJ40443), the National Natural Science Foundation of China (Grant No. 52108099) and the Excellent Youth Project of Education Bureau of Hunan Province, China (Grant No. 21B0134).

## Declarations

**Conflict of interest** The authors declare no conflict of interest.

## References

1. Du, T., Nie, W., Chen, D., Xiu, Z., Yang, B., Liu, Q., Guo, L.: CFD modeling of coal dust migration in an 8.8-meter-high fully mechanized mining face [J]. *Energy* **212**, 118616 (2020). <https://doi.org/10.1016/j.energy.2020.118616>
2. Wang, H., Zhou, S., Liu, Yi., Yihan, Yu., Sha, Xu., Peng, L., Ni, C.: Exploration study on serum metabolic profiles of Chinese male patients with artificial stone silicosis, silicosis, and coal worker's pneumoconiosis [J]. *Toxicol. Lett.* **356**, 132–142 (2021)
3. Yang, X., Haiming, Yu., Zhao, J., Cheng, W., Xie, Y.: Research on the coupling diffusion law of airflow-dust-gas under the modularized airflow diverging dust control technology [J]. *Powder Technol.* **407**, 117703 (2022)
4. Bagnold, R.A.: *The physics of blown sand and desert dunes* [M]. Springer, Netherlands (1941)
5. Roney, J.A., White, B.R.: Estimating fugitive dust emission rates using an environmental boundary layer wind tunnel [J]. *Atmos. Environ.* **40**, 7668–7685 (2006)
6. Kang, L., Guo, L.: Eulerian-Lagrangian simulation of aeolian sand transport [J]. *Powder Technol.* **162**, 111–120 (2006)
7. Liu, Z., Niu, H., Rong, R., Cao, G., He, B.J., Deng, Q.: An experiment and numerical study of resuspension of fungal spore particles from HVAC ducts [J]. *Sci. Total. Environ.* **708**, 134742 (2020)
8. Wang, S., Zhao, B., Zhou, B., Tan, Z.: An experimental study on short-time particle resuspension from inner surfaces of straight ventilation ducts [J]. *Build. Environ.* **53**, 119–127 (2012)
9. Sun, H., Li, A., Long, J., Jifu, Wu.: Experimental study on the characteristics of entrained air during the particle flow fall process [J]. *Powder Technol.* **374**, 421–429 (2020)
10. Sun, H., Li, A., Jifu, Wu., Zhang, J.: Particle flow fall process: a systematic study of entrained air under unconfined and semi-confined fall conditions [J]. *Granular Matter* **22**, 49 (2020)
11. Sun, H., Li, A., Jifu, Wu.: Entrained air by particle plume: comparison between theoretical derivation and numerical analysis [J]. *Part. Sci. Technol.* **39**, 141–149 (2019)
12. Ren, T., Wang, Z., Cooper, G.: CFD modelling of ventilation and dust flow behaviour above an underground bin and the design of

- an innovative dust mitigation system [J]. *Tunn. Undergr. Space Technol.* **41**, 241–254 (2014)
13. Patankar, N.A., Joseph, D.D.: Modeling and numerical simulation of particulate flows by the Eulerian-Lagrangian approach [J]. *Int. J. Multiph. Flow* **27**, 1659–1684 (2001)
  14. Stone, L., Hastie, D., Zigan, S.: Using a coupled CFD-DPM approach to predict particle settling in a horizontal air stream [J]. *Adv. Powder Technol.* **30**, 869–878 (2019)
  15. Witt, P.J., Carey, K.G., Nguyen, T.V.: Prediction of dust loss from conveyors using computational fluid dynamics modelling [J]. *Appl. Math. Model.* **26**, 297–309 (2002)
  16. Torno, S., Toraño, J., Álvarez-Fernández, I.: Simultaneous evaluation of wind flow and dust emissions from conveyor belts using computational fluid dynamics (CFD) modelling and experimental measurements—ScienceDirect [J]. *Powder Technol.* **373**, 310–322 (2020)
  17. Morla, R., Karekal, S., Godbole, A.: CFD simulations of DPM flow patterns generated by vehicles in underground mines for different air flow and exhaust pipe directions [J]. *Int. J. Min. Mineral Eng.* **11**(1), 51–65 (2020)
  18. Hongbo, Xu., Zhang, P., Zhichao, Hu., Mao, E., Yan, J., Yang, H.: Analysis of dust diffusion from a self-propelled peanut combine using computational fluid dynamics [J]. *Biosys. Eng.* **215**, 104–114 (2022)
  19. Wang, Y., Jiang, Z., Zhang, F., Ying, Lu., Bao, Y.: Study on dust diffusion characteristics of continuous dust sources and spray dust control technology in fully mechanized working face [J]. *Powder Technol.* **396**, 718–730 (2022)
  20. Chen, F., Mo, J., Ma, W.: Study on the coupling migration law of airflow-respiratory dust of an 8-m high fully-mechanized mining face [J]. *Energy Explor.* **40**(5), 1360–1381 (2022)
  21. Yin, S., Nie, W., Liu, Q., Hua, Y.: Transient CFD modelling of space-time evolution of dust pollutants and air-curtain generator position during tunnelling [J]. *J. Clean. Prod.* **239**, 117924 (2019)
  22. Guo, L., Nie, W., Yin, S., Liu, Q., Hua, Y., Cheng, L., Cai, X., Xiu, Z., Tao, Du.: The dust diffusion modeling and determination of optimal airflow rate for removing the dust generated during mine tunnelling [J]. *Build. Environ.* **178**, 106846 (2020)
  23. Xiu, Z., Nie, W., Yan, J., Chen, D., Cai, P., Liu, Q., Tao, Du., Yang, Bo.: Numerical simulation study on dust pollution characteristics and optimal dust control air flow rates during coal mine production [J]. *J. Clean. Prod.* **248**, 119197 (2020)
  24. Zhou, G., Zhang, Qi., Baia, R., Fana, T., Wang, G.: The diffusion behavior law of respirable dust at fully mechanized caving face in coal mine: CFD numerical simulation and engineering application [J]. *Process. Saf. Environ. Prot.* **106**, 117–128 (2017)
  25. Fluent, ANSYS, Inc. Release 2020 R2. Ansys fluent theory guide
  26. Sun, H., Li, Z., Long, J., Zeng, L.I.: CFD-DEM coupled calculation of entrained air and particles movement characteristics during particles flow impacting the wall process [J]. *Granular Matter* **24**, 71 (2022)
  27. SpaceClaim, ANSYS, Inc. Release 2020 R2. SpaceClaim documentation
  28. Verduzco, L.F., Horta, J., y Hernández, M.A., Hernández, J.B.: CALRECOD—a software for computed aided learning of REinforced CONcrete structural design [J]. *Adv. Eng. Softw.* **172**, 103189 (2022)
  29. Yaşar, Ö., Uslu, T., Şahinoğlu, E.: Fine coal recovery from washery tailings in Turkey by oil agglomeration [J]. *Powder Technol.* **327**, 29–42 (2017)
  30. Kang, L., Guo, L., Liu, D.: Reconstructing the vertical distribution of the aeolian saltation mass flux based on the probability distribution of lift-off velocity [J]. *Geomorphology* **96**, 1–15 (2008)
  31. Tan, L., Zhang, W., Qu, J., Du, J., Yin, D., An, Z.: Variation with height of aeolian mass flux density and grain size distribution over natural surface covered with coarse grains: a mobile wind tunnel study [J]. *Aeolian Res.* **15**, 345–352 (2014)
  32. Dong, Z., Liu, X., Wang, H., Zhao, A., Wang, X.: The flux profile of a blowing sand cloud: a wind tunnel investigation [J]. *Geomorphology* **49**, 219–230 (2002)
  33. Namikas, S.L.: Field measurement and numerical modelling of aeolian mass flux distributions on a sandy beach [J]. *Sedimentology* **50**, 303–326 (2003)
  34. Fengjun, X., Zhibao, D., Liejin, G., Yueshe, W., Debiao, Li.: Sand particle lift-off velocity measurements and numerical simulation of mass flux distributions in a wind tunnel [J]. *J. Arid. Land* **9**(3), 331–344 (2017)
  35. Hong, W., Wang, B., Zheng, J.: Numerical study on the influence of fine particle deposition characteristics on wall roughness [J]. *Powder Technol.* **360**, 120–128 (2020)
  36. de Almeida Leão, R.X., Amorim, L.S., Martins, M.F., Junior, H.B., Sarcinelli, E., Mesquita, A.L.: A model for velocity streamlines of airborne dust particles spreading caused by free-falling bulk materials [J]. *Powder Technol.* **371**, 190–194 (2020)
  37. Jing, Q., Ferro, A.R., Fowler, K.R.: Estimating the resuspension rate and residence time of indoor particles [J]. *J. Air Waste Manag. Assoc.* **58**(4), 502–516 (2012)

**Publisher's Note** Springer Nature remains neutral with regard to jurisdictional claims in published maps and institutional affiliations.

Springer Nature or its licensor (e.g. a society or other partner) holds exclusive rights to this article under a publishing agreement with the author(s) or other rightsholder(s); author self-archiving of the accepted manuscript version of this article is solely governed by the terms of such publishing agreement and applicable law.